Fidelity Requirements with Fast Transients from VSC-HVdc

Suman Debnath
Oak Ridge National Laboratory
Email: debnaths@ornl.gov

Jingfan Sun
Oak Ridge National Laboratory,
Georgia Institute of Technology

***Abstract*—Fast control afforded by power electronics in high-voltage direct current (HVdc) systems, especially voltage-source converter (VSC) based HVdc systems, needs to be carefully assessed to identify stability boundaries. While there are several averaged models of VSC-HVdc systems that have been studied with low bandwidth alternating current (ac) system models, there have been limited studies to show the need for high-fidelity models to understand the control interactions between different VSC-HVdc systems as well as with other grid components. In this paper, the fidelity of power electronics and connected grid components like transmission lines are identified based on defined use-cases to understand the stability and impact of the fast control afforded by VSC-HVdc systems. These results will be useful to understand the methods required to study control in VSC-HVdc systems.**

***Index Terms*—high-fidelity, power electronics, VSC, HVdc, control, power systems**

I. Introduction

Power electronics in transmission grid like high-voltage direct current (HVdc) systems, flexible alternating current transmission system (FACTS), and other power flow controllers can improve the stability and controllability of existing grids. They also allow economic transfer of power over long distances, connection of asynchronous grids, stable integration of renewable resources, and other benefits. These benefits have led to a number of planning studies like HVdc grids or macrogrids embedded within existing alternating current (ac) transmission systems [1], multi-terminal HVdc (MTdc) systems integrating offshore wind energy [2], and others [3]. Many of these systems are being planned with voltage-source converters (VSCs) like the modular multilevel converter (MMC) [4] with several advanced control functionality being explored. The advanced control functionalities in VSCs need to be carefully assessed to understand their stability boundaries. The careful assessment needs to incorporate the high-bandwidth offered by VSCs. The high-bandwidth offered by VSCs can lead to stability challenges that need to be modeled within the planning studies.

VSCs in HVdc systems like MMCs have been modeling using detailed switch models [5]–[9] or average-value models [7]. While switched system dynamics are not considered in average-value models, these models are much faster to simulate than the detailed switch models. The detailed switch models provide the higher fidelity required to exploit the high-bandwidth offered by VSCs without any approximations (like in the average-value models) that can lead to unstable real system implementations. Along with the higher fidelity identified in VSCs, higher fidelity of components in the transmission ac grid is also of importance.

The transmission line models available in the electromagnetic transient simulation environments can be classified into two categories, i.e., the lumped line model [10]–[14] and distributed line model [15]. The lumped line models, which simplify the system as lumped passive elements in Γ, T, or π circuits [10], perform well under steady state and can be easily translated into state-space representations. While most lumped line models adopt constant values for all frequency range [10]–[12], some modified lumped line models are proposed to introduce frequency dependent effects by constructing pi-equivalent sections with multiple parallel RL-branches [13], [14]. The representation of full frequency dependence of transmission lines are provided by distributed line models, like the Universal Line Model (ULM) [15]. To compare the dynamic response of lumped and distributed line models in MTdc systems, case studies are performed under various scenarios, i.e., step changes in dc voltage reference, ac voltage reference, active power command [11], [14], and fault conditions like line-to-ground fault [12]. However, quantifying the fidelity requirements of transmission lines in advanced HVdc control functionalities that impact the ac grid has not been explored.

In this paper, the fidelity requirements of models used to study HVdc systems with advanced control functionalities is explored. The fidelity requirements include the modeling of VSCs and transmission lines. The use cases considered in these studies include the frequency and voltage control provided by the VSCs. While the first use-case is considered in a MTdc system connecting the various asynchronous interconnections in the United States (US), the second use-case is considered in a modified Kundur two-area system.

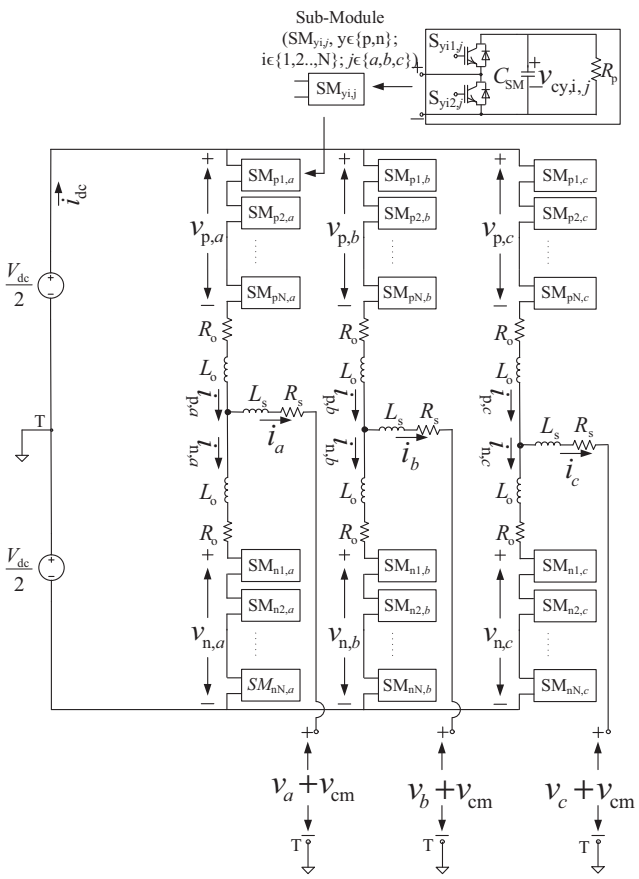

Fig. 1: Circuit diagram of MMC.

II. Modeling of MMCs

To identify the fidelity requirements of VSC-HVdc system, the detailed switching models of converters are necessary to be taken into account. The performance of converter models vary provided that different modeling techniques are applied. In this paper, the modeling technique as explained in [16] is used. MMCs are considered as VSCs in the HVdc systems as they are the most popular topology today. While the analysis has been limited to MMCs, it can be easily extended to other VSCs.

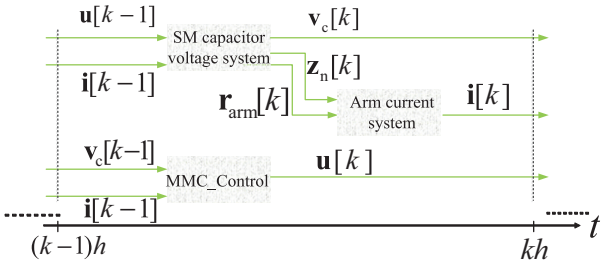

Fig. 2: Summary of MMC-HVdc simulation implementation.

A. Simulation of MMC-HVdc Substation

The circuit diagram of a three-phase MMC is shown in Fig. 1. The basics of operation of the MMC is explained in detail in [4] and is not repeated here.

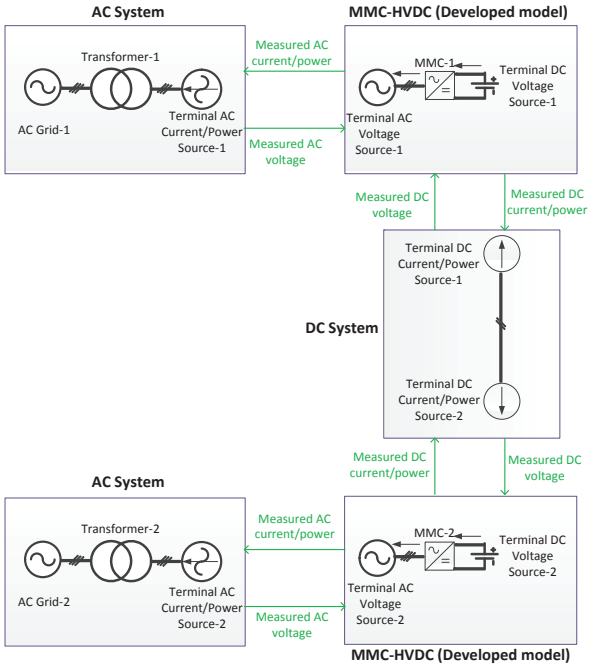

Fig. 3: Summary of simulation algorithm for an example back-to-back MMC-HVdc system.

The high-fidelity modeling of MMC-HVdc system using switched models is computationally expensive to simulate. Hence, advanced simulation algorithm explained in detail in [16] is used to simulate the MMC-HVdc systems. The overall implementation of the MMC-HVdc simulation algorithm is summarized in Fig. 2. In the figure, $\mathbf{v}_c$ refers to the vector consisting of all the SM capacitor voltages, $\mathbf{r}_{arm}$ refers to the vector consisting of $R_{y,j}$, and $\mathbf{i}$ refers to the vector containing all the arm currents. Parallel computation of the SM capacitor voltages is feasible in the SM capacitor voltage system if a multi-core CPU is used.

B. Simulation of Mixed Transmission Systems

The numerical stiffness based parallelization and the corresponding hybrid discretization algorithm proposed to simulate MMCs in mixed transmission in [16] used here. The implementation of this algorithm for a back-to-back MMC-HVdc system connected to two ac grids is shown in Fig. 3.

III. Modeling of Transmission Lines

In addition to the models of MMCs, high fidelity models of the transmission ac and dc grids are also of importance to the analysis of fidelity requirements of VSC-HVdc system. The lumped transmission line model (e.g. π-section model) fails to provide sufficient accuracy when high-frequency transients (higher than 1 kHz) are applied in time-domain analysis. This reduced accuracy at higher frequencies is improved by cascaded lumped line models that have multiple π-sections in series. In general, the greater the number of cascaded π-sections used in the lumped line model, the better is the

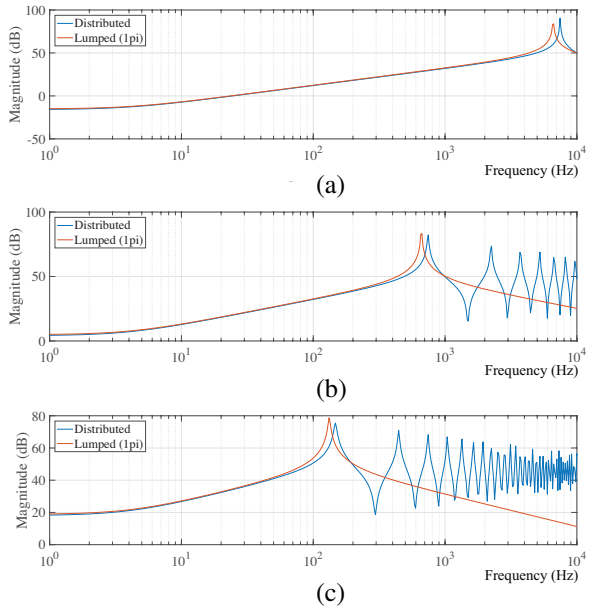

Fig. 4: Frequency response of lumped and distributed transmission line models with different line length: a) 10 km, b) 100 km, and c) 500 km.

accuracy of the model at higher frequencies [12]. The distributed transmission line model is, hereafter, referred to as the distributed line model. While the model fidelity is improved by using many sections, the simulation becomes less efficient due to the increased computational time. This tradeoff should be carefully considered when determining the transmission line model to be used in the analysis.

The length of the transmission line in the system of interest is another important criteria to determine the fidelity of the transmission line model to be used in the analysis. The frequency response of lumped and distributed line models with different line lengths is shown in Fig. 4. It can be observed that the accuracy of the lumped line model decreases with increase in the length of the transmission line [17]. Considering a target frequency of 1 kHz, when the line is longer than 100 km, lumped line model is not sufficiently accurate.

IV. Case-Study I: Voltage Control

The fidelity requirements of VSC-HVdc system are explored through using the models explained in Section II and III. The first case-study is based on a modified Kundur 2-area system [18]. The modification to the original Kundur 2-area system is the replacement of one of the ac lines with a point-to-point HVdc system, as shown in Fig. 5. The two areas in the Kundur 2-area system are connected using a 220 km long 230 kV ac and a $\pm$ 320 kV HVdc transmission lines that are present in parallel to each other. MMCs are deployed as the converter stations on both sides of the point-to-point HVdc line. These MMCs are equipped with two layers of controllers: 1) internal control system to control ac grid currents, dc-link currents, circulating currents, and capacitor voltages, and 2) outer loop ac voltage controller. The outer loop ac voltage controller is enabled at $t = 1$s in this case.

This case-study identifies the need for high-fidelity modeling of transmission lines, as will be shown through results in Section VI. The high-fidelity modeling of VSCs is required to understand the stability of fast control methods developed in VSCs.

A. Internal Control System

The internal control system comprises qd ac-side current control, qd circulating current control of the second- and fourth-order harmonics, 0-component of the circulating current, and the average of all the submodule (SM) capacitor voltages in the MMC. The control system is summarized in Fig. 6 [19]. The detailed description of the internal control system and the SM capacitor voltage balancing strategy can be found in [20].

B. ac Voltage Controller in MMC & Models

The outer-loop ac voltage controller in the MMC is based on an integral control, as shown in Fig. 7.

Outer loop ac voltage controller and phase-locked loop (PLL), whose dynamic interacts with line models, are explicitly modeled as explained below. In this study, the speed of inner controller is assumed to be fast enough (at least 10 times faster than the outer loop controller). This assumption results in a boundary-layer system for the q and d-axis currents. This boundary-layer system is in steady-state with respect to the dynamics of the reduced-order system formed by the outer-loop ac voltage controller.

As shown in Fig. 7, the angular frequency, ω, can be written as

$$\omega = \frac{\mathrm{d}\theta}{\mathrm{d}t} = \omega_{\text{ref}} - K_{\text{pt}} v_{\text{sd}} - \int K_{\text{it}} v_{\text{sd}} \mathrm{d}t. \tag{1}$$

where ω_{ref} is $2\pi \times 60$. K_{pt} and K_{it} are proportional and integrator gains of the PLL compensator, respectively.

Based on the ac voltage controller and the assumption that inner loop controller is fast enough, the q and d-axis ac side currents are

$$\begin{aligned} i_{sq} \approx i_{q\text{ref}} = & K_{p,\text{vdc}}[{v_{\text{c}}^{\Sigma}}^2 - {v_{\text{c,ref}}^{\Sigma}}^2] + \\ & K_{\text{i,vdc}} \int [{v_{\text{c}}^{\Sigma}}^2 - {v_{\text{c,ref}}^{\Sigma}}^2] \mathrm{d}t + i_{sq\text{ref,fd}}, \end{aligned} \tag{2}$$

$$i_{sd} \approx i_{d\text{ref}} = \frac{1}{k_{\text{t}}} \cdot K_{\text{pv}q}(v_{q\text{ref}} - v_{sq}), \tag{3}$$

where $i_{sq\text{ref,fd}} = \frac{P_{\text{dis}}}{3/2 \cdot v_{sq\text{nom}}}$ is the feedforward term of q-axis current. $v_{sq\text{nom}}$ is the nominal value of q-axis ac voltage. v_{c}^{Σ} is the averaged summation of all SM capacitor voltage in one arm of MMC. $K_{\text{p,vdc}}$ and $K_{\text{i,vdc}}$ are proportional and integrator gains of the q-axis controller, respectively. $k_{\text{t}} = 230/330$ is the turns ratio of transformer. $K_{\text{pv}q}$ is the proportional gain of voltage controller.

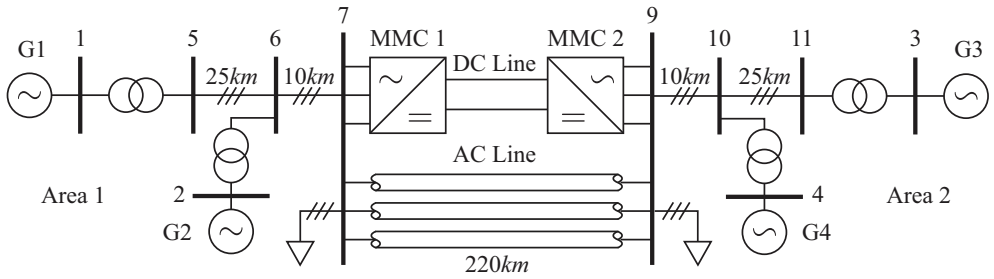

Fig. 5: Single-line diagram of modified Kundur 2-area system.

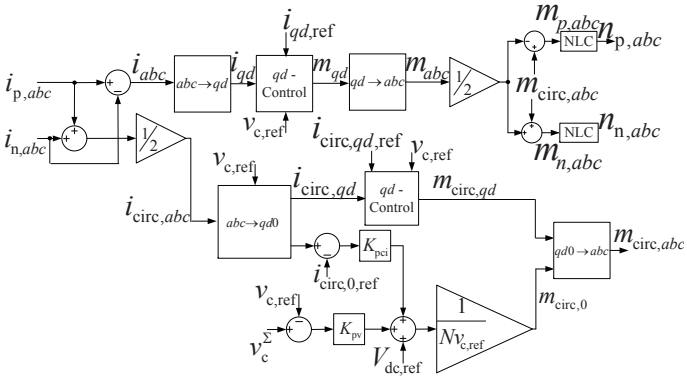

Fig. 6: Summary of internal control system.

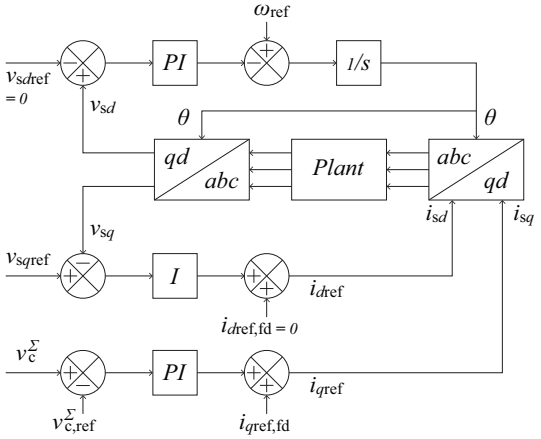

Fig. 7: MMC outer loop controller and PLL.

C. MMC ac-Side Model

The simplified model of the modified Kundur 2-area system (as presented in Fig. 8) is adopted in the small-signal analysis. The ac systems on both sides are simplified into two equivalent ac voltage sources with series impedance. The paralleled ac and dc lines are represented as their lumped line models. Dynamics of the MMCs are considered using the detailed switched-system model explained in Section II. The quantities on MMC1 (rectifier side) and MMC2 (inverter side) sides are marked by r and i, respectively.

The ac-side dynamic model of MMC is depicted by the ac

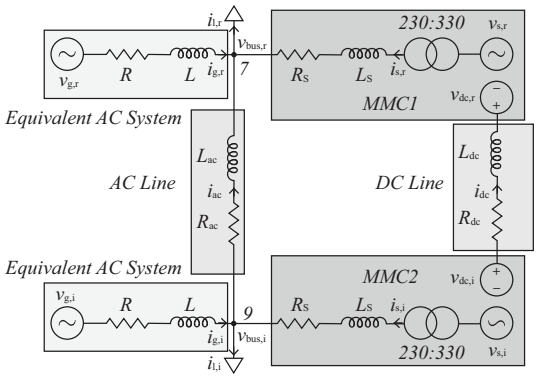

Fig. 8: Simplified model of modified Kundur 2-area system.

side impedance as

$$\begin{aligned} v_{\mathrm{g},abc,\mathrm{k}} - L\frac{\mathrm{d}i_{\mathrm{g},abc,\mathrm{k}}}{\mathrm{d}t} - Ri_{\mathrm{g},abc,\mathrm{k}} \\ = k_{\mathrm{t}} \cdot v_{\mathrm{s},abc,\mathrm{k}} - L_{\mathrm{s}}\frac{\mathrm{d}i_{\mathrm{s},abc,\mathrm{k}}}{\mathrm{d}t} - R_{\mathrm{s}}i_{\mathrm{s},abc,\mathrm{k}}, \end{aligned} \tag{4}$$

where $\mathrm{k} \in \{\mathrm{r},\mathrm{i}\}$ represents either MMC1 or MMC2 side.

Applying the Kirchhoff's Current Law to node 7 and 9 in Fig. 8, the grid side q and d-axis currents, $i_{gqd,k}$, can be substituted by

$$i_{\mathrm{g}qd,\mathrm{k}} = i_{\mathrm{l}qd,\mathrm{k}} - i_{\mathrm{ac},qd,\mathrm{k}} - i_{\mathrm{s}qd,\mathrm{k}}, \tag{5}$$

where $i_{\mathrm{l}qd,\mathrm{k}}$, $i_{\mathrm{ac},qd,\mathrm{k}}$, and $i_{\mathrm{s}qd,\mathrm{k}}$ are the load, ac line, and converter side currents, respectively.

The paralleled ac and HVdc lines connect two ac systems whose phase angles θ are not same. Therefore, The qd quantities on rectifier and inverter side are interpreted in different reference coordinates with different θ. To represent quantities like ac line current $i_{\mathrm{ac},qd,\mathrm{k}}$ in a single reference frame, the the interaction between rectifier and inverter side reference coordinates have to be considered. This transformation is provided in the Appendix A. In this way, (5) can be rewritten as

$$\begin{aligned} i_{\mathrm{g}qd,\mathrm{r}} &= i_{\mathrm{l}qd,\mathrm{r}} - i_{\mathrm{ac},qd,\mathrm{r}} - i_{\mathrm{s}qd,\mathrm{r}} \\ i_{\mathrm{g}qd,\mathrm{i}}\Big|_{\mathrm{i}} &= i_{\mathrm{l}qd,\mathrm{i}}\Big|_{\mathrm{i}} + i_{\mathrm{ac},qd,\mathrm{r}}\Big|_{\mathrm{i}} - i_{\mathrm{s}qd,\mathrm{i}}\Big|_{\mathrm{i}}, \end{aligned} \tag{6}$$

where $i_{\mathrm{ac},qd,\mathrm{r}}\Big|_{\mathrm{i}}$ indicates that the variable $i_{\mathrm{ac},qd,\mathrm{r}}$, which is a

rectifier side variable, is transformed into qd form with the reference coordinate on inverter side.

D. MMC Internal Model

The dynamics of the SM capacitor voltages in the MMC are given by (7).

$$C_{\text{SM}}\frac{\mathrm{d}v_{\text{cx,j,l}}}{\mathrm{d}t} = S_{\text{x,j,l}}i_{\text{x,j}}, \forall \text{x} \in \{\text{p,n}\}, \text{j} \in \{\text{a,b,c}\}, \text{l} \in [1,\text{n}]. \quad (7)$$

Summing up all SM capacitor voltages in six arms, the dynamic model of the averaged arm voltage, v_{c}^{Σ}, is

$$6C_{\text{SM}}\frac{\mathrm{d}v_{\text{c}}^{\Sigma}}{\mathrm{d}t} = 2Nm_{\text{circ},0}i_{\text{dc}} - N\frac{\frac{3}{2}v_{sq}i_{sq}}{v_{\text{c}}^{\Sigma}}, \quad (8)$$

where $m_{\text{circ},0}$ is the zero component circulating modular index represented by

$$m_{\text{circ},0} = \frac{1}{Nv_{\text{c,ref}}}\Big[V_{\text{dc,ref}} - K_{\text{pc}}\big(\frac{P_{\text{dis}}}{3V_{\text{dc,ref}}} - \frac{i_{\text{dc}}}{3}\big)\Big], \quad (9)$$

where $V_{\text{dc,ref}}$ and $v_{\text{c,ref}}$ are reference value of dc link voltage and SM capacitor voltage, respectively. P_{dis} is the dispatch command of the converter. K_{pc} is the gain of droop controller.

E. ac & dc Transmission Lines

The transmission line dynamics are defined based on lumped line models in this section. These models indicate the approximate position of poles of the overall system with the proposed control. The approximate position of poles will be used to identify if lumped lines can sufficiently capture the dynamics of the system.

The ac line dynamic can be expressed as

$$v_{\text{bus},abc,\text{i}} - v_{\text{bus},abc,\text{r}} = R_{\text{ac}}i_{\text{ac},abc} + L_{\text{ac}}\frac{\mathrm{d}i_{\text{ac},abc}}{\mathrm{d}t}. \quad (10)$$

Applying the technique in Appendix A, the ac transmission line dynamics in (10) is transformed with reference coordinate on rectifier side as

$$\begin{aligned} v_{\text{bus},qd,\text{i}}\Big|_{\text{r}} - v_{\text{bus},qd,\text{r}}\Big|_{\text{r}} = R_{\text{ac}}i_{\text{ac},qd}\Big|_{\text{r}} + L_{\text{ac}}\frac{\mathrm{d}i_{\text{ac},qd}}{\mathrm{d}t}\Big|_{\text{r}} \\ + \omega L_{\text{ac}}i_{\text{ac},dq}\Big|_{\text{r}} + \omega\Big|_{\text{r}}L_{\text{ac}}i_{\text{ac},dq,\text{nom}}. \end{aligned} \quad (11)$$

The dc transmission line is modeled as

$$L_{\text{dc}}\frac{\mathrm{d}i_{\text{dc}}}{\mathrm{d}t} + R_{\text{dc}}i_{\text{dc}} = -v_{\text{dc,r}} + v_{\text{dc,i}}. \quad (12)$$

F. Small-Signal Model of Modified Kundur 2-Area System

The small-signal model of the modified Kundur 2-area system is obtained by linearizing the system dynamics equations (4), (8), (11), and (12). This linearized model is thereafter transformed to the Laplace domain to obtain the corresponding state-space representation given by

$$\mathbf{A}(\text{s})\mathbf{X}(\text{s}) = \mathbf{0}, \quad (13)$$

where the matrix $\mathbf{A}$ can be calculated based on the dynamics of state variables. The state vector $\mathbf{X}(\text{s})$ is

$$\mathbf{X}(\text{s}) = [\text{V}_{sq,\text{r}}, \text{V}_{sd,\text{r}}, \text{V}_{\text{c,r}}^{\Sigma}, \text{V}_{sq,\text{i}}, \text{V}_{sd,\text{i}}, \text{V}_{\text{c,i}}^{\Sigma}, \text{I}_{\text{ac},q,\text{r}}, \text{I}_{\text{ac},d,\text{r}}, \text{I}_{\text{dc}}]^{-1}. \quad (14)$$

The solution of (13) gives the poles for the system.

$$\det(\mathbf{A}(\text{s})) = 0. \quad (15)$$

V. Case-Study II: Frequency Control

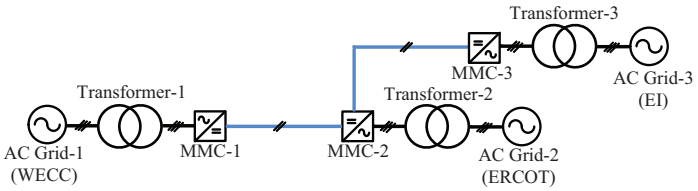

Fig. 9: Multi-terminal MMC-HVdc system connected three ac grids.

The second case-study considered in this paper is a multi-terminal MMC-HVdc (MTdc) system connected to three asynchronous ac grids, as shown in Fig. 9. The use case in this case-study explores the frequency support that the MTdc system can provide to the asynchronous grids. The frequency support results in sharing of primary reserves between the different grids, reducing the reserve requirements in each asynchronous grid [21]. The MMC-HVdc links connected to the ac grids provide primary frequency support based on smart autonomous control (SAC). Some of the events considered to impact frequency include changes in the power processed by the MMCs, loss of generator(s) in the ac grid, loss of loads, and others. The proposed SAC provides the primary response to the frequency events that have occurred. The relocation of power resources between the ac grids, or the secondary response to the frequency events, is implemented by the central energy management system (EMS). The central EMS also sends power dispatch commands based on load-generation forecasting and economics.

In SAC, each MMC behaves like an agent in a multi-agent control implementation. In each agent, the following layers of control are present: (i) internal control system to control ac grid currents, dc-link currents, circulating currents, and capacitor voltages that is explained in Section IV-A, (ii) ac frequency control, and (iii) dc-link voltage control.

A. ac Frequency & dc Voltage Control

Expert systems are designed to support ac-side frequency during major frequency incursions. The ac-side frequency is estimated based on digital implementation of synchronous reference frame phase-locked loop (SRF-PLL) [22]. The SRF-PLL uses the measured ac-side voltages as input.

The expert systems vary the average capacitor voltage and active power during frequency incursions to provide inertial and governor response (like generators). While the variation in the average capacitor voltage is effected during changes in commanded power, the active power is varied during significant frequency events like loss of generators or loads. The frequency disruption observed during change in commanded power is particular noticeable in a weak grid.

The expert system developed to provide the inertial support using the average capacitor voltage is shown in Fig. 10. If the estimated frequency is greater than the dead-band setting and there was a change in the commanded power from the central

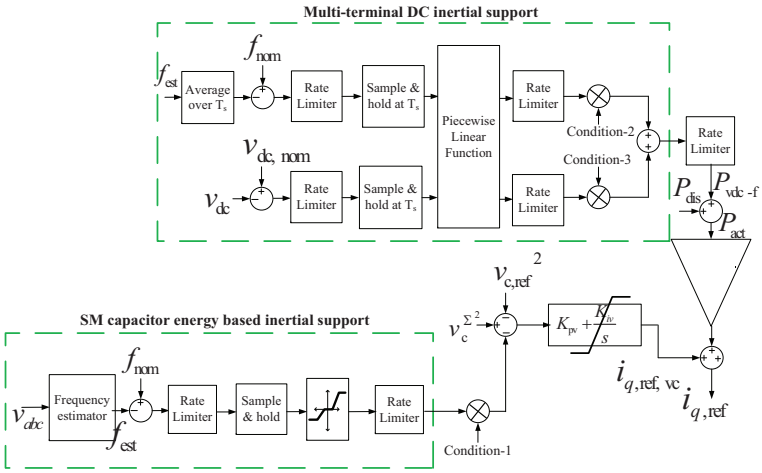

Fig. 10: Summary of inertial support.

EMS, the average capacitor voltage reference is varied based on the estimated frequency. That is, if the estimated frequency is below a particular threshold frequency, the SM capacitor voltage is reduced and energy is supplied to the ac grid without impacting the power flow in the dc terminals. Similarly, if the estimated frequency is above a particular threshold frequency, the SM capacitor voltage is increased and energy is removed from the ac grid. The aforementioned thresholds determine the dead-band used on the estimated frequency to avoid spurious events detection. In the dead-band, the SM capacitor voltage is controlled based on description in Section IV-A.

Based on a dead-band setting on the estimated frequency and if there is no change in the commanded power, the loss of generator or load is assumed. In this scenario, the q-axis ac-side current reference is added to another component based on the change in the frequency. Similarly, the reference to the 0-component of the circulating current is varied based on the estimated frequency to maintain net-zero power between the ac and dc sides. Since, the MMC is connected in a multi-terminal configuration, the change in power reference at only one MMC terminal will impact the dc-link voltage. To maintain the stability of the dc system, the other MMCs have to react to the change in power at one of the MMC terminals. Therefore, there is a provision to detect the loss of generators or loads in the ac grid connected to the other MMC terminals through the dc-link voltage.

Based on a dead-band setting on the dc-link voltage and if the connected ac grid's frequency is within the dead-band settings, the q-axis ac-side current and 0-component of the circulating current are varied based on the measured dc-link voltage. If both the dc-link voltage and the connected ac grid's frequency is beyond their respective dead-band settings, then the q-axis ac-side current and the 0-component of the circulating current are varied based on both the measured dc-link voltage and estimated ac-side frequency. The control system to provide inertial support using the active power is summarized in Fig. 10.

To evaluate the proposed SAC system in planning process, high-fidelity models of VSCs and transmission lines are required as will be noticed in the next section. The use of average-value models of VSCs will not be sufficient to understand stability of the proposed SAC, especially with the fast control capabilities that MMC-type systems can offer. Specifically, the switched system dynamics are a necessity to evaluate the boundaries with fast advanced control implementations on MMCs. The high-bandwidth of these controllers also necessitate the need for high-fidelity transmission line models.

VI. Simulation Results

The two case-studies explained in Sections IV and V are simulated in this section to quantify the benefits of fidelity requirements.

A. Voltage Control

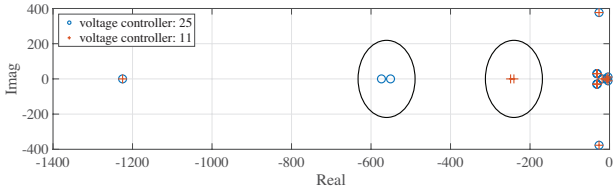

Fig. 11: Poles of the modified Kundur 2-area system with different ac voltage controller gains.

The poles of the modified Kundur 2-area system calculated by solving (15) are shown in Fig. 11. All the poles are located in the left-half plane, which means that the system is stable. Depending upon the form of the outer-loop ac voltage controller, the poles in the system may be high negative values. These values result in the fast controller, which can interact with the ac-side components like transmission line. If the ac-side transmission lines are modeled using lumped line model, the interactions may not be adequately captured. Hence, to achieve greater accuracy with advanced VSC functionalities

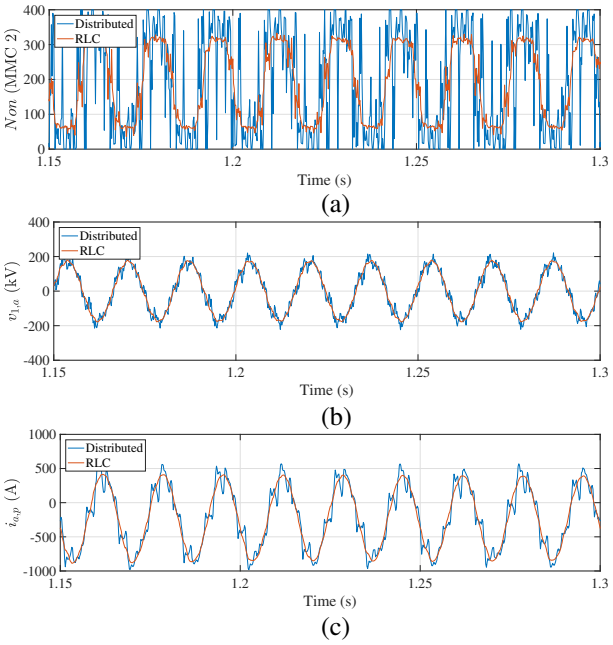

Fig. 12: Simulation of Kundur 2-area system with lumped and distributed line models: a) MMC 1 phase A upper arm N_{on}, and b) MMC 1 phase A instantaneous voltage.

(like fast voltage control), detailed frequency-dependent distributed line model should be used. These assessments are verified by PSCAD simulation results provided in Fig. 12, where the study system with lumped line model fails to capture the rapid oscillation observed in the case of the study system with the distributed line model. Based on these results, the ac transmission line models considered in the next section are based on distributed line models.

B. Frequency Control

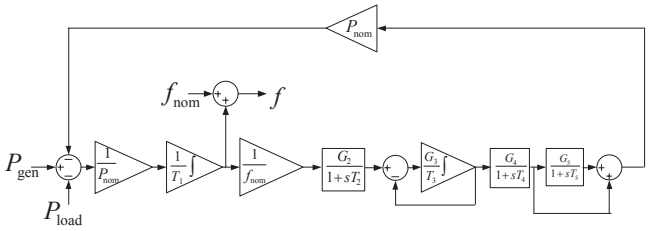

Fig. 13: ac grid model in WECC.

In this section, the MTdc system shown in Fig. 9 is assumed to be connected Eastern Interconnection (EI), Electric Reliability Council of Texas (ERCOT), and Western Electric Coordinating Council (WECC) grids. The MMC parameters have been mentioned in [16]. The models of the asynchronous grids are developed based on National Energy Reliability Council (NERC) data available [21]. While second-order dynamic system models are sufficient to represent the ac grids in EI and ERCOT, the ac grid in WECC required advanced models based on WSEIG1 [23] to accurately represent the frequency data available. The ac grid models for EI and ERCOT are given by

$$F(s) = F_{\text{nom}}(s) + \frac{G}{1 + 2\frac{\delta}{\omega_n}s + \frac{s^2}{\omega_n^2}}\left(P_{\text{gen}} - P_{\text{load}}\right), \quad (16)$$

where F and F_{nom} are the actual and nominal values of the frequency of ac grid, respectively, P_{gen} and P_{load} are the generated and consumed power, respectively, and the rest are parameters of the second-order dynamic system model. The corresponding ac grid model for WECC is shown in Fig. 13.

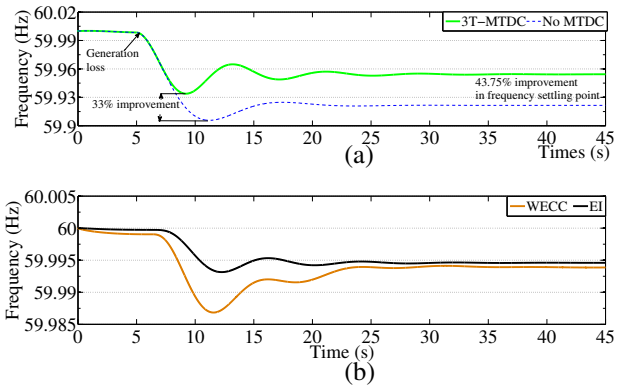

Fig. 14: Loss of generation in ERCOT: (a) Comparison of frequency in ERCOT with and without MTdc, (b) Response of EI and WECC when frequency is shared using MTdc.

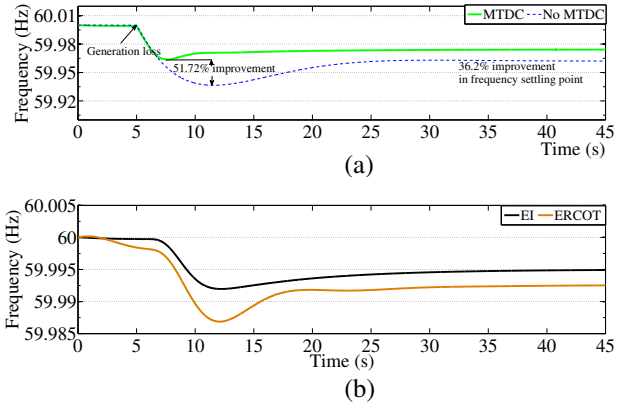

Fig. 15: Loss of generation in WECC: (a) Comparison of frequency in WECC with and without MTdc, (b) Response of EI and ERCOT when frequency is shared using MTdc.

Two cases are considered to study the impact of the proposed control strategy: (i) 500 MW generation loss in ERCOT, and (ii) 500 MW generation loss in WECC. The corresponding results are shown in Figs. 14-15. The presence of the MTdc improves the primary frequency response in each interconnection by up to 51.75%, as noticed in Figs. 14(a)-15(a). The improvement is noticed in the frequency nadir and settling point. When one interconnection losses generation, the other interconnections' frequency is also impacted because the MTdc enables sharing of the frequency deviations between the interconnections. The aforementioned sharing of frequency can be noticed through the impact on other interconnections

in Figs. 14(b)-15(b). Without the high-fidelity models used in this section, much slower controllers will need to be used for conservative stability estimates with average-value models. The slower control system reduces the improvements by up to 50% in the frequency sharing between the asynchronous grids.

VII. Conclusions

The high-fidelity models of VSCs and transmission lines are reviewed in this paper and are analyzed in two case-studies. The two case-studies considered here evaluate advanced control functionalities in VSCs like ac-side voltage and frequency control methods. The requirements for switched-system VSC models and the frequency-dependent distributed parameter transmission line models are identified through these two case-studies. The frequency control case-study also shows the benefits of connected asynchronous grids in the US with up to 51.75% improvement in the frequency response. The improved frequency response can reduce the primary reserves that need to be maintained in each asynchronous grid.

Acknowledgment

This paper and the work described were sponsored by the U.S. Department of Energy (DOE) Office of Electricity Delivery and Energy Reliability (OE) Transformers and Advanced Components (TRAC) under the Grid Modernization Laboratory Consortium. The authors acknowledge Dr. Yuri Markarov and Dr. Marcelo Elizondo of Pacific Northwest National Laboratory, and Dr. Madhu Chinthavali of Oak Ridge National Laboratory, for their valuable inputs in this work. Authors also would like to thank Dr. Kerry Cheung who leads the DOE TRAC program for establishing the project concept, advancing implementation, and providing ongoing guidance.

Appendix A
qd/abc Transformation between Different Reference Coordinates

The qd quantities in rectifier and inverter are in different reference coordinates. In this case, $\theta_\mathrm{r} = \omega_\mathrm{ref} t + \phi_\mathrm{r}$, $\theta_\mathrm{i} = \omega_\mathrm{ref} t + \phi_\mathrm{i}$. θ_r and θ_i have the same angular frequency ω but different initial phase shift ϕ.

Given a variable $i_{q,\mathrm{i}}$ in qd form from θ_i, to transform it into qd of θ_r, the following transformations can be used.

$$
\begin{aligned}
T_r &= \frac{2}{3}\begin{bmatrix}[C_\mathrm{r}] & [C_\mathrm{r}-] & [C_\mathrm{r}+] \\ [S_\mathrm{r}] & [S_\mathrm{r}-] & [S_\mathrm{r}+]\end{bmatrix}, \\
T_\mathrm{i}^{-1} &= \begin{bmatrix}[C_\mathrm{i}] & [S_\mathrm{i}] \\ [C_\mathrm{i}-] & [S_\mathrm{i}-] \\ [C_\mathrm{i}+] & [S_\mathrm{i}+]\end{bmatrix}
\end{aligned}
\tag{A.1}
$$

$$
\begin{aligned}
\begin{bmatrix} i_{q,\mathrm{r}} \\ i_{d,\mathrm{r}} \end{bmatrix} &= T_\mathrm{r} \cdot T_\mathrm{i}^{-1} \begin{bmatrix} i_{q,\mathrm{i}} \\ i_{d,\mathrm{i}} \end{bmatrix} \\
&= \frac{2}{3}\begin{bmatrix}[C_\mathrm{r}] & [C_\mathrm{r}-] & [C_\mathrm{r}+] \\ [S_\mathrm{r}] & [S_\mathrm{r}-] & [S_\mathrm{r}+]\end{bmatrix} \cdot \begin{bmatrix}[C_\mathrm{i}] & [S_\mathrm{i}] \\ [C_\mathrm{i}-] & [S_\mathrm{i}-] \\ [C_\mathrm{i}+] & [S_\mathrm{i}+]\end{bmatrix} \cdot \begin{bmatrix} i_{q,\mathrm{i}} \\ i_{d,\mathrm{i}} \end{bmatrix} \\
&= \begin{bmatrix}[C_\mathrm{diff}] i_{q,\mathrm{i}} - [S_\mathrm{diff}] i_{d,\mathrm{i}} \\ [S_\mathrm{diff}] i_{q,\mathrm{i}} + [C_\mathrm{diff}] i_{d,\mathrm{i}}\end{bmatrix}
\end{aligned}
\tag{A.2}
$$

where $C_\mathrm{diff} = \cos(\theta_\mathrm{r} - \theta_\mathrm{i})$ and $S_\mathrm{diff} = \sin(\theta_\mathrm{r} - \theta_\mathrm{i})$.

References

[1] MISO, "Transmission expansion plan," 2014.

[2] J. Lin, "Integrating the first hvdc-based offshore wind power into pjm system – a real project case study," *IEEE Transactions on Industry Applications*, vol. 52, no. 3, pp. 1970–1978, May 2016.

[3] M. A. Elizondo, R. Fan, H. Kirkham, M. Ghosal, F. Wilches-Bernal, D. A. Schoenwald, and J. Lian, "Interarea oscillation damping control using high voltage dc transmission: a survey," *IEEE Transactions on Plasma Science*, pp. 1–1, 2018.

[4] S. Debnath, J. Qin, B. Bahrani, M. Saeedifard, and P. Barbosa, "Operation, control, and applications of the modular multilevel converter: A review," *IEEE Transactions on Power Electronics*, vol. 30, no. 1, pp. 37–53, Jan 2015.

[5] U. Gnanarathna, A. Gole, and R. Jayasinghe, "Efficient modeling of modular multilevel hvdc converters (MMC) on electromagnetic transient simulation programs," *IEEE Transactions on Power Delivery*, vol. 26, no. 1, pp. 316–324, Jan 2011.

[6] F. Yu, W. Lin, X. Wang, and D. Xie, "Fast voltage-balancing control and fast numerical simulation model for the modular multilevel converter," *IEEE Transactions on Power Delivery*, vol. 30, no. 1, pp. 220–228, Feb 2015.

[7] H. Saad, S. Dennetiere, J. Mahseredjian, P. Delarue, X. Guillaud, J. Peralta, and S. Nguefeu, "Modular multilevel converter models for electromagnetic transients," *IEEE Transactions on Power Delivery*, vol. 29, no. 3, pp. 1481–1489, June 2014.

[8] F. Ajaei and R. Iravani, "Enhanced equivalent model of the modular multilevel converter," *IEEE Transactions on Power Delivery*, vol. 30, no. 2, pp. 666–673, April 2015.

[9] T. Maguire, B. Warkentin, Y. Chen, and J. Hasler, "Efficient techniques for real time simulation of mmc systems," in *International Conference on Power Systems Transients*, July 2013.

[10] T. Dhaene and D. de Zutter, "Selection of lumped element models for coupled lossy transmission lines," *IEEE Transactions on Computer-Aided Design of Integrated Circuits and Systems*, vol. 11, no. 7, pp. 805–815, jul 1992.

[11] M. Sriram and S. Kang, "Efficient approximation of the time domain response of lossy coupled transmission line trees," *IEEE Transactions on Computer-Aided Design of Integrated Circuits and Systems*, vol. 14, no. 8, pp. 1013–1024, 1995.

[12] N. R. Chaudhuri, R. Majumder, B. Chaudhuri, and J. Pan, "Stability analysis of VSC MTDC grids connected to multimachine AC systems," *IEEE Transactions on Power Delivery*, vol. 26, no. 4, pp. 2774–2784, oct 2011.

[13] J. Beerten, S. D. Arco, and J. Suul, "Cable model order reduction for HVDC systems interoperability analysis," in *11th IET International Conference on AC and DC Power Transmission*. Institution of Engineering and Technology, 2015.

[14] J. Beerten, J. A. Suul, and S. D. Arco, "Frequency-dependent cable modelling for small-signal stability analysis of VSC-HVDC systems," *IET Generation, Transmission & Distribution*, vol. 10, no. 6, pp. 1370–1381, apr 2016.

[15] A. Morched, B. Gustavsen, and M. Tartibi, "A universal model for accurate calculation of electromagnetic transients on overhead lines and underground cables," *IEEE Transactions on Power Delivery*, vol. 14, no. 3, pp. 1032–1038, jul 1999.

[16] S. Debnath and M. Chinthavali, "Numerical stiffness based simulation of mixed transmission systems," *IEEE Transactions on Industrial Electronics*, pp. 1–1, 2018.

[17] W. Wang, O. Marjanovic, and M. Barnes, "Droop control modelling and analysis of multi-terminal HVDC for offshore wind farms," in *10th IET International Conference on AC and DC Power Transmission (ACDC 2012)*. Institution of Engineering and Technology, 2012.

[18] M. Klein, G. Rogers, and P. Kundur, "A fundamental study of inter-area oscillations in power systems," *IEEE Transactions on Power Systems*, vol. 6, no. 3, pp. 914–921, 1991.

[19] S. Debnath and M. Chinthavali, "Control of MMC-HVDC in low-inertia weak grids," in *2017 IEEE 12th International Conference on Power Electronics and Drive Systems (PEDS)*. IEEE, dec 2017.

[20] S. Debnath and M. Chinthavali, "MMC-HVDC: Simulation and control system," in *2016 IEEE Energy Conversion Congress and Exposition (ECCE)*. IEEE, sep 2016.

[21] N. R. Subcommittee, *Balancing and Frequency Control*. North American Electric Reliability Corporation, January 2011.

[22] S. Golestan, J. M. Guerrero, and J. C. Vasquez, "Three-phase plls: A review of recent advances," *IEEE Transactions on Power Electronics*, vol. 32, no. 3, pp. 1894–1907, March 2017.

[23] G. Kou, P. Markham, S. Hadley, T. King, and Y. Liu, "Impact of governor deadband on frequency response of the u.s. eastern interconnection," *IEEE Trans. Smart Grid*, vol. 7, no. 3, pp. 1368–1377, May 2016.